Beating effect between a thermoacoustic source and its mechanical partner

Kai Wang,[1,2] Daming Sun,[1,a)] Jie Zhang,[1] Ning Zhang,[1] Kai Luo,[1] and Limin Qiu[1]

[1)] *Institute of Refrigeration and Cryogenics, Zhejiang University, Hangzhou, 310027, China*

[2)] *Energy Research Institute @ NTU, Nanyang Technological University, Singapore 637141*

(Dated: 14 December 2015)

Beating effects between a thermoacoustic source and its mechanical partner-a piston-spring oscillator are numerically predicted and experimentally observed in the free-decay process. Through analyzing the indicator diagram, periodic energy transfer characteristics between thermoacoustic source and its mechanical partner during the beating oscillation is revealed and analyzed. The oscillation frequency is found to split into two modes intrinsically even when the resonance frequencies are initially tuned to be the same. The patterns and frequencies of the beating oscillations are sensitively affected by the characteristics of acoustic sources. The study sheds light on the underlying mechanisms of beating oscillations occurred in thermoacoustic systems with multiple resonant sub-units.

[a)] Author to whom correspondence should be addressed. Electronic mail:sundaming@zju.edu.cn

I. INTRODUCTION

Thermoacoustic effect refers to thermal and acoustical interactions of compressible fluid leading to conversions between thermal and acoustic energies. In recent years, great efforts have been made to take advantages of thermoacoustic effects for converting heat into mechanical power by thermoacoustic engines.[1–7] Simple acoustic networks formed by several pipes rather than reciprocating mechanical pistons are adopted in thermoacoustic engines. The absence of mechanical moving parts in thermoacoustic engines brings them the advantages of simple structures, low costs, and high reliability. Up to now, traveling-wave thermoacoustic engines have achieved the highest efficiency up to 41% of Carnot efficiency[8] and acoustic power up to tens of kilowatts,[9–11] showing a promising prospect in energy conversion fields.

Thermoacoustic engine is essentially an acoustic resonant system that is composed of distributed acoustic inertance and compliance as well as dissipative and source components. When the acoustic source-regenerator is exposed to a large temperature gradient, the resonant system becomes acoustically unstable and generates spontaneously oscillation which finally grows to a saturated state. In order to extract the generated acoustic power, thermoacoustic engine is typically connected with acoustoelectric convertors which are mechanically resonant systems formed by moving mass and springs, such as linear alternators,[12,13] loudspeakers,[14,15] etc. In this case, two or even more acoustic resonant sub-units interact with each other while operate independently to some extent in the meantime in the combined system. The acoustic oscillations become much more complex due to the combined effects of the independent and interactive operations of these sub-units.

Unstable pressure oscillation with periodical variation of amplitude may occur in thermoacoustic systems with multiple resonant sub-units. The phenomenon is known as beating effect in acoustics,[16] which is referred to as the superposition of two sound waves of slightly different frequencies. The envelope of the superposed waves is in a sinusoidal oscillation, the frequency of which is the difference between the two sound wave frequencies, i.e. so-called beating frequency. One of the simplest beating oscillations occurs in two mass-spring oscillators connected with a soft spring.[17] In solid materials, the atoms not only oscillate around their equilibrium positions but also interact with each other, resulting in the similar phenomenon.[17–19] Beating effect has been widely applied in acoustics, such as acoustic

signal detections and analysis.[20,21] Recently, they were also observed in Stirling engine,[22] Rijke tube,[23] and premixed combustor,[24] which introduced harmful instabilities to the system operations.

In this study, we firstly report on the beating effects between a traveling-wave thermoacoustic engine and a piston-spring mechanical oscillator. Unstable beating oscillations are observed in the free decay processes of the coupled system. Different from the simple coupled mass-spring oscillators which can be analyzed by lumped parameter method,[17] the thermoacoustic engine is an acoustic oscillator which has distributed acoustic parameters and acoustic source terms from the regenerator. The coupling between the thermoacoustic engine and the mechanical oscillator is thus more complex and informative in consideration of the energy conversion process in the regenerator. The internal mechanism and factors that affect the patterns and frequencies of the beating oscillations are then studied numerically and experimentally. Furthermore, beating effect occurs when the system is in a free decay process and the acoustic intensity is very weak. It may be an ideal chance to study the internal detailed parameters of the regenerators, such as intrinsic frequency and very small inhomogeneity of regenerator matrix, since the weak intrinsic characteristics will show up more apparently at this moment.

II. EXPERIMENTAL APPARATUS

The experimental apparatus consists of a traveling-wave thermoacoustic engine[25] and a piston-spring mechanical oscillator,[7] as depicted in Fig. 1. The traveling-wave thermoacoustic engine mainly consists of a hot heat exchanger (HHX), a regenerator, a main ambient heat exchanger (MAHX), a secondary ambient heat exchanger (2nd AHX) and several tube components. The dimensions of the thermoacoustic engine are listed in Table I. The combinations of the tubes form a resonant acoustic network which has an almost constant resonant frequency. The regenerator in the looped tube is the key component where energy conversion occurs, and therefore is the excitation source for the thermoacoustic oscillations when a sufficiently large temperature gradient is applied along it. The MAHX and 2nd AHX are both of shell-and-tube type with working gas flowing inside the thin stainless steel tubes and chilling water flowing across the tubes bundles. The inner diameters of the thin tubes are 3 mm. The numbers of the tubes in MAHX and 2nd AHX are 187 and 199, respectively. The

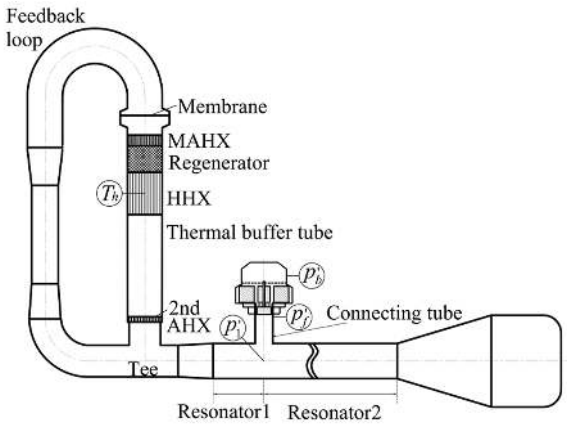

FIG. 1. Thermoacoustic source and its mechanical partner-a piston-spring oscillator.

HHX is of fin type with a porosity of 0.361 and the fin spacing is 1 mm. The regenerator is filled with stainless steel screens with a porosity of 0.777 and a hydraulic radius of 52.4 μm.

The mechanical oscillator, which is actually the mechanical part of a linear alternator, is connected at the resonator through connecting tube.[25] It mainly consists of a moving piston, a spring connected to the piston, and a back volume. The piston of the mechanical oscillator can be driven by a linear motor. A ball valve is set near the far end of the connecting tube to control the external excitations. The parameters of the mechanical resonator are given in Table II. Helium at 1.2 MPa is used as the working gas, and the dynamic pressures are measured by PCB piezoelectric pressure sensors (102B15), as denoted by p_1', p_f' and p_b', respectively. The resonant frequency of the mechanical oscillator at the above filling pressure is 66.88 Hz.

III. NUMERICAL MODEL AND METHOD

A time-domain network thermoacoustic model[25] is adopted for the traveling-wave thermoacoustic engine in the numerical simulations. The basic equations for the duct components, including tubes and heat exchangers, are written as,

$$\frac{\partial p'}{\partial x} = -l\frac{\partial U'}{\partial t} - r_\nu U' \tag{1}$$

TABLE I. Geometric parameters of traveling-wave thermoacoustic engine and the grid number used in simulation.

Component		Diameter,m	Length,m	Grid
MAHX		0.09	0.03	2
Regenerator		0.09	0.074	10
HHX		0.09	0.12	2
Thermal buffer tube		0.1	0.291	7
2nd AHX		0.1	0.02	1
Tube under 2nd AHX		0.09	0.126	3
Feedback loop	Tube near tee	0.09	0.295	5
	Cone	/	0.095	2
	Tube	0.076	0.28	6
	Cone	/	0.1	2
	Tube above MAHX	0.1	0.7027	10
Resonator Part	Tube near tee	0.09	0.095	2
	Cone	/	0.1	2
	Resonator 1	0.1	0.145	2
	Connecting tube	0.05	0.48	6
	Resonator 2	0.1	2.155	22
	Cone	/	1.31	11
	Tube	0.261	0.52	5

TABLE II. Parameters of mechanical oscillator.

Parameter	Value
Moving mass M, kg	1.097
Spring stiffness K, N/m	1.89×10^{5}
Mechanical resistance R_m,N·s/m	5
Piston area A_m, m^2	1.9635×10^{-3}
Back volume V_b, m^3	1.63×10^{-3}

$$\frac{\partial U'}{\partial x} = -c\frac{\partial p'}{\partial t} - \frac{1}{r_\kappa}p' \tag{2}$$

where p' and U' are the dynamic pressure and the volume flow rate, respectively; x and t are the axial coordination and the time. l, c, r_ν, and r_κ are the acoustic inertance, acoustic compliance, acoustic resistance, and thermal-relaxation resistance per unit length, respectively,[26]

$$l = \frac{\rho_0}{A}\frac{1 - \mathrm{Re}[f_\nu]}{|1 - f_\nu|^2} \tag{3}$$

$$c = \frac{A}{\gamma p_0}\left(1 + (\gamma - 1)\,\mathrm{Re}[f_\kappa]\right) \tag{4}$$

$$r_\nu = \frac{\omega\rho_0}{A}\frac{\mathrm{Im}[-f_\nu]}{|1 - f_\nu|^2} \tag{5}$$

$$r_\kappa = \frac{\gamma}{\gamma - 1}\frac{p_0}{\omega A \mathrm{Im}[-f_\kappa]} \tag{6}$$

where p_0, ρ_0 and ω are mean pressure, mean gas density and angular frequency, respectively; A and γ denote cross-sectional area and specific heat ratio. Re[ ] and Im[ ] denote the real and imaginary parts of a complex parameter, respectively. The f_κ and f_ν are spatially averaged complex viscous and thermal-relaxation functions, respectively. For circular tubes with diameter $D = 4r_h$, where r_h is the hydraulic radius, such as ducts and AHXs,[26]

$$f_{\kappa,\nu} = \frac{4J_1\left[0.5(i-1)D/\delta_{\kappa,\nu}\right]}{J_0\left[0.5(i-1)D/\delta_{\kappa,\nu}\right](i-1)D/\delta_{\kappa,\nu}} \tag{7}$$

where $\delta_{\kappa,\nu}$ denotes the thermal or viscous penetration depth.[26] For parallel plates with spacing $2y_0 = 2r_h$, such as HHX,[26]

$$f_{\kappa,\nu} = \frac{\tanh\left[(1+i)y_0/\delta_{\kappa,\nu}\right]}{\left[(1+i)y_0/\delta_{\kappa,\nu}\right]} \tag{8}$$

The control equations for the regenerator are given by,

$$\frac{\partial p'}{\partial x} = -\frac{\rho_0}{\phi A}\left[1 + \frac{(1-\phi)^2}{2(2\phi - 1)}\right]\frac{\partial U'}{\partial t} - \frac{1}{2}\frac{f}{r_h\phi^2A^2}\rho_0|U'|U' \tag{9}$$

$$\frac{\partial U'}{\partial x} = -c\frac{\partial p'}{\partial t} - \frac{1}{r_\kappa}p' + \mathrm{Re}[g]U' + \frac{\mathrm{Im}[g]}{\omega}\frac{\partial U'}{\partial t} \tag{10}$$

where ϕ denotes the porosity of the regenerator matrix. g and f are complex source term and friction factor of the regenerator, and are defined by,

$$g = \frac{f_\kappa - f_\nu}{(1 - f_\kappa)(1 - Pr)} \frac{1}{T_0} \frac{\mathrm{d}T_0}{\mathrm{d}x} \tag{11}$$

$$f = \frac{1268 - 3545\phi + 2544\phi^2}{R_e} + (-2.82 + 10.7\phi - 8.6\phi^2) \tag{12}$$

where Pr is the Prandtl number, and the Reynolds number $R_e = 4|U'|r_h\rho_0/(\mu_0\phi A)$. Eq. (11) is the critical term that accounts for the energy conversion in the regenerator. The temperature gradient term in Eq. (11) determines the intensity of the energy conversion effect.

The dynamic characteristics of the mechanical oscillator are simulated using the following equations,

$$\frac{\mathrm{d}X'}{\mathrm{d}t} = v' \tag{13}$$

$$\frac{\mathrm{d}p'_b}{\mathrm{d}t} = \frac{\gamma p_0 A_m}{V_b} v' \tag{14}$$

$$\frac{\mathrm{d}v'}{\mathrm{d}t} = \frac{1}{M}(p'_f A_m - p'_b A_m - R_m v' - KX') \tag{15}$$

where X' and v' are the displacement and velocity of the piston; p'_f and p'_b are the dynamic pressures in front of the piston and the back volume, respectively. As the AC motor of the mechanical oscillator is electrically open-circuited in the damping process, the electromagnetic force on the piston does not need to be included. To start up an initial pressure oscillation before the damping, the velocity of the piston is given with a specific value, which will be mentioned in the following sections.

According to the forms of the control equations for the thermoacoustic engine and the mechanical oscillators, the whole system can be equivalently converted into a dynamic network system, as shown in Fig. 2. The equivalent pistons with mechanical resistances represent the acoustic inertances and resistances, and the lossy volumes between the pistons represent the compliance and thermal relaxation losses. Due to the thermoacoustic conversion effect, the regenerator has source terms.

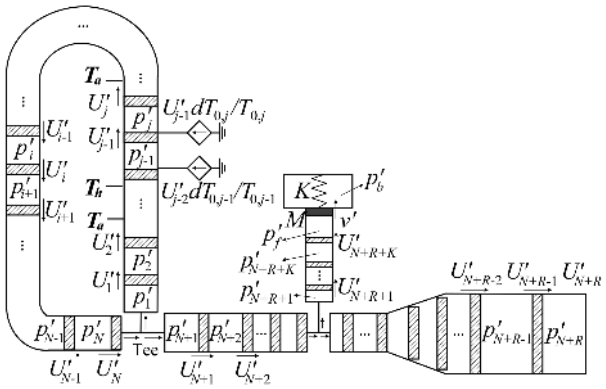

FIG. 2. Schematic of discretized equivalent network of the thermoacoustic engine and mechanical oscillator coupled system.

The control equations for the duct components are then discretized into the following forms,

$$\frac{\mathrm{d}U_i'}{\mathrm{d}t} = -\frac{1}{l_i \delta x_i}(p_{i+1}' - p_i' + r_{\nu,i}\delta x_i U_i') \tag{16}$$

$$\frac{\mathrm{d}p_i'}{\mathrm{d}t} = -\frac{1}{c_i \delta x_i}(U_i' - U_{i-1}' + \frac{1}{r_{\kappa,i}}\delta x_i p_i') \tag{17}$$

The treatments of the control equations of the grids near the connecting position of the engine and the mechanical oscillator are critical for the acoustic coupling. The gas near the piston is assumed to move synchronously with the same velocity of v' as the piston. Therefore, the pressure oscillation p_f' in the discretized volume in front of the piston is expressed as,

$$\frac{\mathrm{d}p_f'}{\mathrm{d}t} = -\frac{1}{c_i \delta x_i}(v' A_m - U_{N+R+K}' + \frac{1}{r_{\kappa,i}}\delta x_i p_f') \tag{18}$$

Similarly, the volume flow for the duct grid $i = N + R + K$ in front of the piston is discretized as,

$$\frac{\mathrm{d}U_i'}{\mathrm{d}t} = -\frac{1}{l_i \delta x_i}(p_f' - p_i' + r_{\nu,i}\delta x_i U_i') \tag{19}$$

The pressure oscillation of the grid $i = N + R + K$ is controlled by the same equation as the other duct components, as given in Eq. 17. N, R and K in the above equations denote the total grid numbers of the loop, the resonator part and the branched connecting tube, respectively. In this way, the mechanical oscillator can be easily coupled to the acoustic field.

The control equations for the regenerator are discretized as,

$$\frac{\mathrm{d}U'_j}{\mathrm{d}t} = -\frac{\phi A_j}{\rho_{0,i}\delta x_j\left[1+\frac{(1-\phi)^2}{2(2\phi-1)}\right]}\left(p'_{j+1}-p'_j+\frac{\rho_{0,j}|U'_j|f_j\delta x_j}{2r_h\phi^2A_j^2}\right) \tag{20}$$

$$\frac{\mathrm{d}p'_j}{\mathrm{d}t} = -\frac{1}{c_j\delta x_j}\left(U'_j-U'_{j-1}+\frac{1}{r_{\kappa,j}}\delta x_j p'_j-\mathrm{Re}[g_j]U'_{j-1}-\frac{\mathrm{Im}[g_j]}{\omega}\frac{\mathrm{d}U'_{j-1}}{\mathrm{d}t}\right) \tag{21}$$

The number of grids of each component of the thermoacoustic engine are listed in Table I for which the grid-independence has been validated. A set of first-order differential equations can be obtained by combining the control equations for all the grids of the thermoacoustic engine and the mechanical oscillator, and numerically solved using the Matlab ODE45 solver[27] with given initial conditions. An initial angular frequency should be first guessed to calculate the coefficients for the governing equations, and then the calculated oscillation angular frequency is used in the following iterations to get the final results.

IV. RESULTS AND DISCUSSIONS

A. Free-decay oscillation of stand-alone thermoacoustic engine

Fig. 3 shows the free-decay oscillation of the stand-alone thermoacoustic engine, which is first numerically simulated and experimentally measured. In the experiments, a stable oscillation is first established by the external excitation from the reciprocating piston driven by an AC linear motor operating at the resonant frequency of the thermoacoustic engine, i.e. about 65 Hz. Then, the ball valve is closed rapidly to isolate the thermoacoustic engine from the excitation source, leaving it into free-decay oscillation. The treatments of the free-decay oscillation of thermoacoustic engine in the simulations have the similar procedure and the same boundary conditions as the experiment. When no other resonant system is connected with it, the thermoacoustic engine is an independent acoustic resonant system with only the gas resonator. As shown in Fig. 3, both the simulated and measured oscillations show the same variation trends and attenuate exponentially as no temperature gradient is applied to compensate the acoustic dissipations, which mainly result from the viscous frictions and thermal-relaxation effects. The spectrum analysis shows that the oscillation energy is focused on only one frequency, i.e. 64.38 Hz in the simulation and 64.35 Hz in the experiment. The decaying speed of the envelope of the oscillation indicates the intensity of

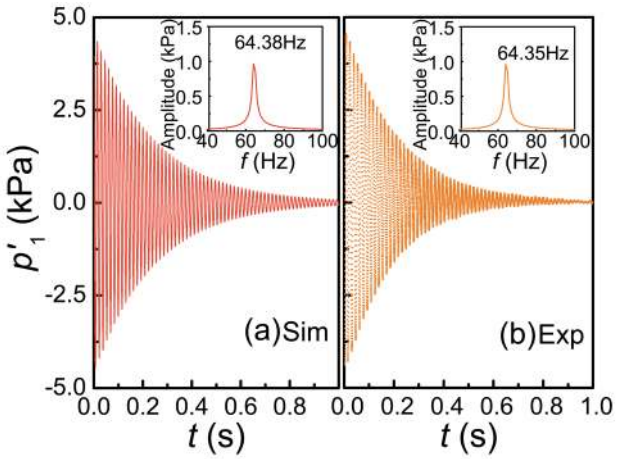

FIG. 3. Free-decay oscillation of thermoacoustic engine when the heating temperature is 292 K (a) Simulation (b) Experiment.

acoustic dissipations in the acoustic resonant system, and is usually adopted as an effective way to determine the quality factor.[25]

B. Beating oscillation of coupled system

1. Beating oscillation waveforms

When the mechanical oscillator is connected with the thermoacoustic engine, the coupled system has two resonant mechanisms, including the long gas resonator and the mechanical oscillator. Driven by the curiosity about the characteristics of the quality factor of the coupled system, the free-decay oscillations of the coupled system are then measured and simulated to get the decaying curves. To achieve the free-decay oscillation of the combined system, the piston is first driven sinusoidally at a peak velocity of 1 m/s by a linear motor to excite an initial acoustic field. The power supply of the linear motor is then switched off rapidly to let the combined system oscillate freely when the acoustic field becomes stable. The electric circuit of the motor is thus open-circuited and no electromagnetic force is applied on the mechanical oscillator. To start the same process in the simulation, the velocity of the piston is set as the same as that in the experiments, and then the forced excitation is removed to simulate the coupled free-decay oscillation of the whole system.

The obtained pressure oscillations in the two resonant sub-units coupled system are com-

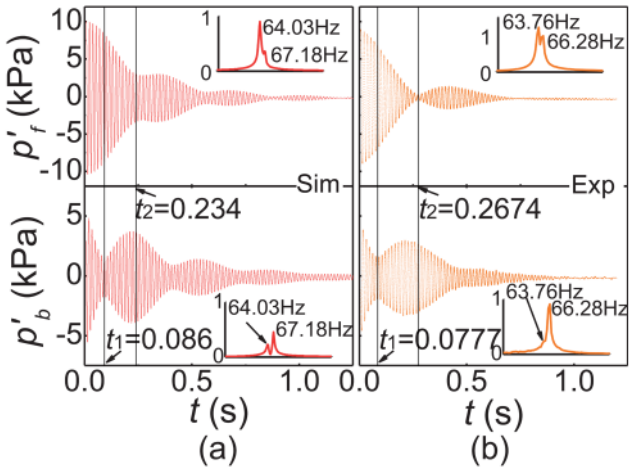

FIG. 4. Beating effect of thermoacoustic source and piston-spring oscillator coupled system when the heating temperature is fixed at 292 K. (a) Simulation (b) Experiment.

pletely different from that of the stand-alone thermoacoustic engine, as shown in Fig. 4 when the heating temperature is kept at ambient temperature. The dynamic pressures in front and the back volume of the mechanical resonator don't experience smooth attenuation any more but periodical amplitude variations, as illustrated by p'_f and p'_b, respectively. Two frequencies with a slight difference are found to exist simultaneously in the oscillations. The above unique features of the oscillations indicate that beating oscillation occurs when the thermoacoustic engine and mechanical oscillator are coupled together. The envelope curves of the dynamic pressures p'_f and p'_b beat at the frequencies of 3.15 Hz in the simulation and 2.52 Hz in the experiments, which are exactly the differences of the two split frequencies. The spectrum analysis of the pressure waveform p'_f in front of the mechanical oscillator shows that the oscillation energy is more focused on the lower frequency, i.e. 64.03 Hz in simulation, and 63.76 Hz in experiment. The higher frequencies are found dominant in the back volume of mechanical resonator, as shown by spectrum diagrams of p'_b. The patterns of the beating oscillations in the simulation and the experiment are similar. As the minor losses in the flow channels, the loss from the membrane, and the gas leakage loss across the piston are not included in the numerical model, the losses in the simulations are underestimated compared to that in the practical system.[25] Therefore, the decay speed in the experiment is a little faster than that in the simulation, resulting in a smaller number of beats.

When the heating temperature is increased to 353 K with the room temperature of 292

K, the simulated and experimentally observed beating oscillations are illustrated in Fig. 5. Due to the established temperature gradient in the regenerator and the excited oscillating flows, the gas particles can generate acoustic power inside the regenerator. The energy dissipations in the system are therefore partly compensated by the acoustic power generation from thermoacoustic effect in the regenerator, as indicated mathematically by the source term g in Eq. 11. As a result, the decaying speeds are a little slower and larger numbers of beats are observed. Besides, the two fundamental frequencies of the beating oscillations at 353 K differ slightly from those at 292 K. The spectrum analyses indicate that the intensities of lower fundamental frequency become more dominant over those of the higher one, compared to the relationships of the relative intensities of the two frequencies in Fig. 4. Considering that the only difference of the operating conditions between Fig. 4 and Fig. 5 is the heating temperature, it is obvious that the enhancement of spectrum energy of the lower fundamental frequency at 353 K is induced by the thermoacoustic energy conversion of the thermoacoustic engine. The higher fundamental frequency component is correspondingly controlled by the mechanical oscillator. It is observed in Fig. 5 that the intensity of the lower frequency is higher than that of the higher frequency in the back volume in the simulation while they are in an inverse relationship in the experiment. This is because the losses in the simulation is lower than that in the experiment and the heating temperature of 353 K is much closer to the calculated onset point than the experimental one, which are 487.5 K and 508.1 K respectively. Thus, the lower frequency induced by the energy conversion effect shows relatively stronger intensity in the simulation. The intensity of the higher frequency component still keeps stronger than that of the lower frequency one in the back volume in the experiment. Simulations and measurements are also conducted at even higher heating temperatures, as shown in Fig. 6, when the heating temperature is 474 K. The intensity of the lower fundamental frequency component increases with the heating temperature, and becomes so strong that it almost covers the higher one in the simulation. The intensity of the lower frequency component in the experiment also grows to be much stronger than the higher one. The lower frequency component in the back volume in the experiments becomes dominant over the higher one too, due to the enhanced energy conversion effect induced by the larger temperature gradient. When increasing the heating temperature above the onset point, only one frequency component is observed and the beating oscillation is almost invisible, showing the dominant contribution of the thermoacoustic source.

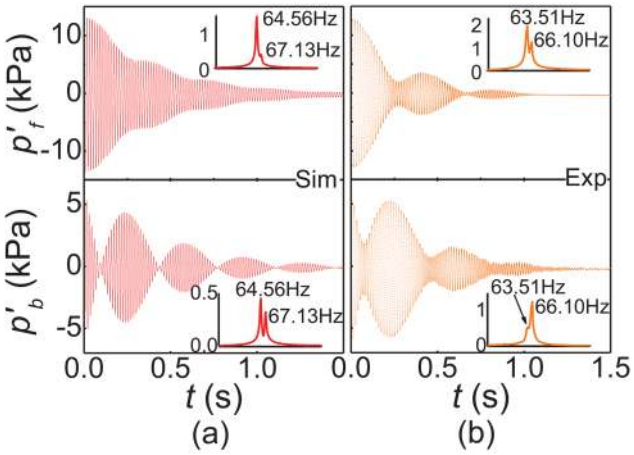

FIG. 5. Beating effect of thermoacoustic source and piston-spring oscillator coupled system when the heating temperature is fixed at 353 K. (a) Simulation (b) Experiment.

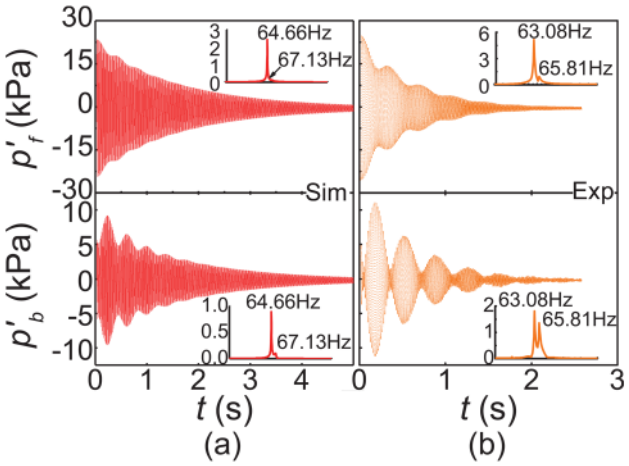

FIG. 6. Beating effect of thermoacoustic source and piston-spring oscillator coupled system when the heating temperature is fixed at 474 K. (a) Simulation (b) Experiment.

2. Energy transfer characteristics

The variations of beating oscillations of p'_f and p'_b show inverse tendencies during the free-decay oscillations in both simulations and experiments. The rapid falling of the amplitude of p'_f is always accompanied by the dramatic increase of the amplitude of p'_b, and vice versa, as shown in Figs. 4-6. Strong interactions are involved between the two resonant sub-units. The force-displacement $F - X'$ indicator diagrams of the piston are depicted in Fig. 7. The time nodes are denoted in consistent with those in Fig. 4. F is defined as the force acting on the

working gas from the piston with downwards as the positive direction, which is calculated by $-p'_f A_m$. The displacement X' of the piston is calculated according to the dynamic pressure p'_b in the back volume using the relation of $X' = p'_b V_b/\gamma p_0 A_m$, with downwards as the positive direction. If the indicator diagram is traced in the clockwise direction, net work is done by the piston; otherwise net work is done on the piston. Fig. 7 gives the simulated and tested indicator diagrams when the heating temperature is fixed at 292 K. As illustrated, the indicator diagram goes in clockwise direction during the time interval of t_0-t_1, indicating that the mechanical oscillator is doing net work on the thermoacoustic engine. The area encircled by the curves in the indicator diagram, which denotes the energy transfer rate, gradually shrinks. The dynamic pressure p'_b in the back volume as well as the displacement X' of the piston decrease rapidly as the energy is extracted to the engine. However, the energy transferring rate is not enough to compensate the dissipating rate in the engine operating at the large externally-driven amplitude. The pressure in the thermoacoustic engine during this period is decaying but with a slow rate especially at the initial stage when the energy transferring rate is the largest, as shown in Fig. 4. After the time node of t_1 when the dynamic pressure p'_b in the back volume reaches its first local minimum, the indicator diagram turns in the reverse direction in both the simulation and the experiment, indicating that energy is transferring back to the mechanical oscillator from the thermoacoustic engine. Consequently, the oscillation in the thermoacoustic engine damps quickly until it reaches the local minimum at t_2 when the energy transfer direction is then reversed back again. With the combined effects of the externally imported energy and the internal losses of the mechanical oscillator, the piston displacement shows a tendency of an increase during most of the period and then a slightly decrease near t_2. After the time node of t_2, a part of the energy stored in the mechanical oscillator is then transferred back to the thermoacoustic engine once again. The above process occurs repeatedly until all the oscillation energy is dissipated through the losses from both the resonant sub-units. The analysis of the indicator diagram reveals that oscillation energy alternates between two resonant sub-units in the coupled system, and causes the pressure amplitudes to vary periodically.

To clearly reveal the energy transfer characteristics during the beating oscillations, the instantaneous energies stored in the thermoacoustic engine and the mechanical oscillator are calculated based on the simulated pressure and volume flow data. The instantaneous acoustic energy stored inside the thermoacoustic engine $E_{TE}(t)$ is the sum of the kinetic

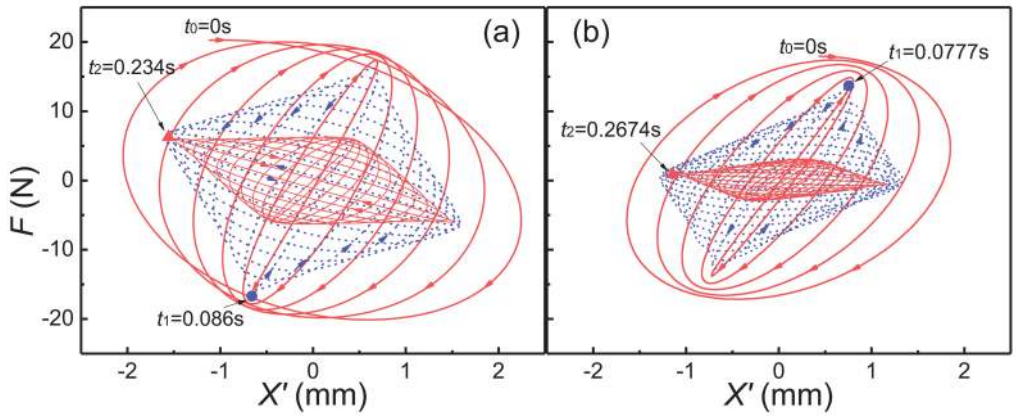

FIG. 7. Indicator diagram $F - X'$ during beating when the heating temperature is 292 K (a) Simulation (b) Experiment. The lines in red denote net positive work is done by the piston while those in blue denote net negative work. First three time intervals of the interactions between thermoacoustic engine and mechanical oscillator are illustrated here, including t_0-t_1, t_1-t_2, and the period after t_2.

energy from the gas motion and the potential energy from the compression of the gas of every discretized grid, as expressed by,[16]

$$E_{TE}(t) = \sum_i \frac{1}{2}\left[\rho_{0,i}\left(\frac{U_i'}{A_i}\right)^2 + \frac{p_i'^2}{\gamma p_0}\right]V_i \tag{22}$$

where V_i is the gas volume of the discretized grid. The energy storage in the mechanical oscillator $E_{LA}(t)$ is the sum of the kinetic energy from the moving mass and the potential energies from the mechanical spring and the gas compression in the back volume,

$$E_{LA}(t) = \frac{1}{2}Mv'^2 + \frac{1}{2}KX'^2 + \frac{1}{2}\frac{p_b'^2}{\gamma p_0}V_b \tag{23}$$

The total energy stored in the combined system $E_{total}(t)$ is defined as the sum of the energies inside the thermoacoustic engine and the mechanical oscillator,

$$E_{total}(t) = E_{TE}(t) + E_{LA}(t) \tag{24}$$

The calculated energy storage levels of the beating oscillations at different heating temperatures are given in Fig. 8. As shown, the energy storages in the thermoacoustic engine and the mechanical oscillator vary periodically with a reverse phase while the total stored energy decays exponentially with a much smooth tendency. It clearly indicates that the energy

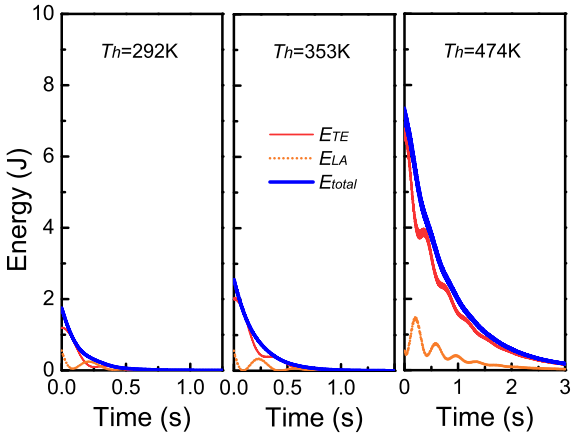

FIG. 8. Energy storage levels of the oscillations vs. time at different heating temperatures in simulations.

is periodically alternating between the thermoacoustic engine and its mechanical partner, as also analyzed from the characteristics of the pressure waveforms previously. When the heating temperature increases, due to the positive energy conversion of the regenerator, the attenuation rate of the total energy storage decreases from 7.147 Np/m at 292 K to 4.865 Np/m at 353 K, and only 1.341 Np/m at 474 K , which are fitted by $E_{total}(t) = E_{total}(0)e^{-\lambda t}$. The energy storage level in the thermoacoustic engine goes up remarkably, while that in the mechanical oscillator has very limited enhancement. When the heating temperature is increased to 474 K, the energy storage in the engine becomes so dominant that it takes up more than 70% of the total energy storage.

The above phenomenon indicates that the thermoacoustic engine is actually an active acoustic resonant system which has positive energy generation compensating for the losses, while its partner-the mechanical oscillator is a passive resonant system with only lossy mechanisms. When the acoustic power generation effect in the thermoacoustic engine becomes sufficiently strong, the energy emission from the mechanical resonator is so weak compared to its partner that it only passively follows the acoustic oscillation generated by thermoacoustic engine. As a result, the beating effect becomes less obvious, and even vanishes when the coupled system reaches self-started state above the onset point. Therefore, beating effect is only observable when the coupled resonant sub-units have comparable energy levels.

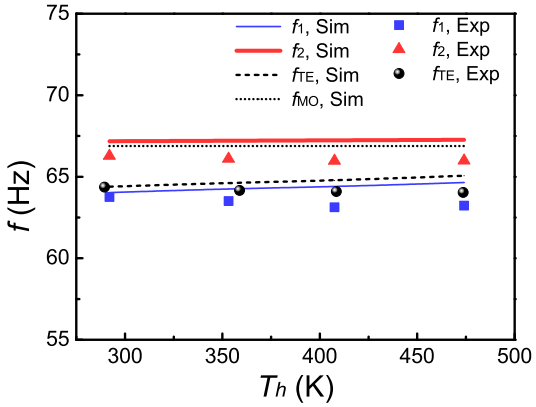

FIG. 9. Relationships between the beating oscillation frequencies and the resonant frequencies of the thermoacoustic engine and mechanical oscillator. f_1 and f_2 denote the frequencies of the beating oscillation; f_{TE} and f_{MO} are resonant frequencies of thermoacoustic engine and mechanical oscillator, respectively.

3. Effects of heating temperature on distributions of beating frequencies

The relationships between the beating oscillation frequencies and the resonant frequencies of the thermoacoustic engine and mechanical oscillator at different heating temperatures are given in Fig. 9. As shown, the two adjacent frequencies f_1 and f_2 of the beating oscillations are distributed closely along the resonant frequencies f_{MO} and f_{TE} of the mechanical oscillator and the thermoacoustic engine respectively. The lower frequency f_1 follows the tendency of the resonant frequency f_{TE} of the thermoacoustic engine with a little smaller value, while the higher one f_2 is just above the resonant frequency f_{MO} of the mechanical oscillator. It verifies again that the lower frequency is contributed by the thermoacoustic engine while the higher one derives from the mechanical oscillator, as analyzed before. When the two resonant systems with similar energy levels are coupled, the generated oscillation spontaneously splits into two adjacent frequency modes which can be figured out by their resonant frequencies respectively. In general, the heating temperature doesn't have much influence on the frequency distributions.

4. *Effects of resonant frequencies on beating frequencies*

The beating oscillation frequencies have been clarified to be closely related to the resonant frequencies of the thermoacoustic engine and the mechanical oscillator. It is worth investigating if it is possible to eliminate the beating effect in the coupled system by tuning the two resonant frequencies to be the same. The effects of the factors that affect the resonant frequencies on the beating effect are then studied, including the moving mass M and the spring stiffness K of the mechanical oscillator, and the resonator tube length L_r of the thermoacoustic engine. The resonant frequency f_{TE} of the thermoacoustic engine is measured with the free-decay oscillation method by exciting an initial acoustic field. The calculated resonant frequency f_{TE} is obtained in the same way by using the above numerical model. The resonant frequency of the mechanical oscillator f_{MO} is dependent on the gas spring in the back volume, the spring stiffness and the moving mass, with the relation of $f_{MO} = \sqrt{\left(K + \gamma p_0 A_m^2 / V_b\right) / M}/(2\pi)$. It is difficult to accurately measure the resonant frequency at a filling pressure as any sealed volume in front of the piston will add extra gas spring effect. Due to the simplicity of the mechanisms affecting the resonant frequency, only the calculated resonant frequency of the mechanical oscillator is presented.

Fig. 10 shows the variations of the beating frequencies and the resonant frequencies of the sub-units when adjusting the moving mass M, the spring stiffness K, and resonator tube length L_r, respectively. As shown in Fig. 10(a), the resonant frequency f_{MO} of of the mechanical oscillator significantly decreases with the moving mass M, which further greatly affects the distributions of the beating oscillation frequencies f_1 and f_2. However, it is illustrated that the coupled oscillation always splits into two frequencies at whatever moving mass M. The beating oscillation still exists even when the resonant frequencies of the thermoacoustic engine and the mechanical oscillator reach the same value of 64.4 Hz by adjusting the moving mass M to 1.183 kg. The beating oscillation frequencies f_1 and f_2 tend to approach the resonant frequencies respectively at relatively large and small moving masses M when the resonant frequency of the mechanical oscillator is far away from that of the thermoacoustic engine. Similar trends are also observed when adjusting the spring stiffness K and the resonator tube length L_r, as shown in Figs. 10(b) and (c). The beating oscillation frequencies are always distributed on the up and down sides of the resonant frequencies[17]. It shows that the beating oscillation always occurs in the thermoacoustic

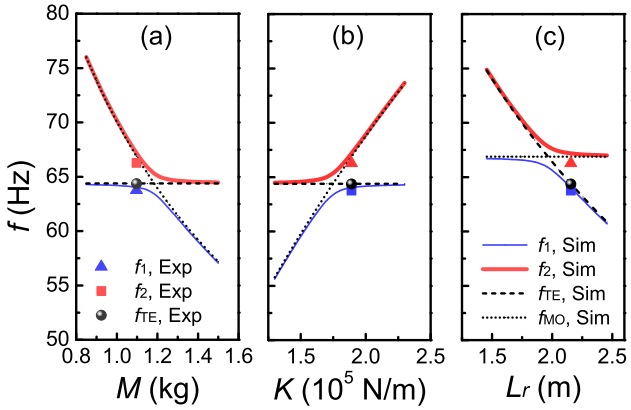

FIG. 10. Effects of (a) moving mass M (b) spring stiffness K and (c) resonator length L_r on beating oscillation frequencies when the heating temperature is fixed at 292 K.

engine and the mechanical oscillator coupled system even when the resonant frequencies of both sub-units are tuned to be the same.

Even though the beating phenomenon still takes place even if the thermoacoustic engine and the mechanical oscillator are tuned, the resonant frequency of the thermoacoustic engine will be dominant at temperatures well above the onset temperature and make the beat almost unobservable. It should be noted that the tuning of the resonant frequencies are still essential for many thermoacoustic systems coupled with acoustoelectric converters to maximize the conversion efficiency of the acoutoelectric converters as well as the overall efficiency of the coupled system.[12,28–32]

V. CONCLUSION

We have firstly observed beating effects in free-decaying oscillations between a thermoacoustic engine and a mechanical oscillator. The oscillation characteristics and energy conversion processes of the beating phenomenon are investigated both numerically and experimentally. In the free-decaying process of a stand-alone thermoacoustic engine, the oscillation attenuates exponentially and smoothly. Whereas, periodical unstable beating oscillations between two frequencies occur when a piston-spring mechanical oscillator is coupled with the thermoacoustic engine. The different patterns of the beating oscillations and the relative intensities of the two frequency components at different heating temperatures indicate that

the beating oscillation is strongly affected by the energy conversion in the regenerator. The analyses from the indicator diagrams show clearly that the oscillation energy is alternating between the engine and the mechanical oscillator periodically. The coupled oscillations are found to split into two adjacent frequencies which are closely related to the resonant frequencies of the engine and mechanical oscillator. It even happens when the two resonant frequencies are tuned to be the same by adjusting the moving mass, spring stiffness, and resonator tube length. The beating effect is an intrinsic phenomenon in the coupled multiple resonant sub-units which have comparable levels of energy levels. When one of the resonant sub-units has a more powerful energy generation mechanism over the other one, the one with a weak energy level will be passively driven by it. Then the oscillation in the coupled system is concentrated on only one frequency and the beating oscillation vanishes. The study may shed lights on the unstable beating oscillations occurred in double-acting thermoacoustic systems and Stirling engines with multiple resonant sub-units, which have been reported to have seriously deteriorated the performances. Besides, since the beating frequencies and oscillation patterns are sensitively affected by the energy conversion of the regenerator, it may also provide an opportunity to distinguish the tiny differences between regenerators.

ACKNOWLEDGMENTS

The work was supported by National Natural Science Foundation of China under contract No. 51476136 and China Postdoctoral Science Foundation under contract No. 2013M541772. The authors acknowledge Professor A.T.A.M. de Waele at Eindhoven University of Technology for the helpful discussions.

REFERENCES

[1]S. Backhaus and G. W. Swift, Nature **399**, 335 (1999).

[2]C. Olivier, G. Penelet, G. Poignand, and P. Lotton, J. Appl. Phys. **115**, 174905 (2014).

[3]D. M. Sun, K. Wang, Y. Xu, Q. Shen, X. J. Zhang, and L. M. Qiu, J. Appl. Phys. **111**, 094905 (2012).

[4]K. Tang, T. Lei, and J. Tao, J. Appl. Phys. **112**, 094909 (2012).

[5]M. Nouh, O. Aldraihem, and A. Baz, J. Sound Vib. **333**, 3138 (2014).

[6]A. T. A. M. de Waele, J. Sound Vib. **325**, 974 (2009).

[7]K. Wang, D. M. Sun, J. Zhang, Y. Xu, J. Zou, K. Wu, L. M. Qiu, and Z. Y. Huang, Appl. Energy (2015).

[8]M. E. H. Tijani and S. Spoelstra, J. Appl. Phys. **110**, 093519 (2011).

[9]J. J. Wollan, G. W. Swift, S. N. Backhaus, and D. L. Gardner, in *AIChE Meeting* (New Orleans, LA, USA, 2002).

[10]G. W. Swift and J. Wollan, GasTIPS , 21 (2002).

[11]B. Arman, J. Wollan, V. Kotsubo, S. Backhaus, and G. W. Swift, in *13th International Cryocooler Conference* (Kluwer Academic/Plenum, New Orleans, Louisiana, 2004).

[12]D. M. Sun, K. Wang, X. J. Zhang, Y. N. Guo, Y. Xu, and L. M. Qiu, Appl. Energy **106**, 377 (2013).

[13]Z. H. Wu, L. M. Zhang, W. Dai, and E. C. Luo, Appl. Energy **124**, 140 (2014).

[14]Z. B. Yu, A. J. Jaworski, and S. Backhaus, Appl. Energy **99**, 135 (2012).

[15]H. F. Kang, P. Cheng, Z. B. Yu, and H. F. Zheng, Appl. Energy **137**, 9 (2015).

[16]T. D. Rossing, "Springer handbook of acoustics," (Springer, 2007).

[17]L. D. Landau and E. M. Lifshitz, "Mechanics, second edition," (Pergamon Press, 1969).

[18]Y. C. Zhang, S. W. Song, C. F. Liu, and W. M. Liu, Phys. Rev. A **87**, 023612 (2013).

[19]J. Y. Vaishnav and C. W. Clark, Phys. Rev. Lett. **100**, 153002 (2008).

[20]F. Gao, Y. J. Zheng, X. H. Feng, and C. D. Ohl, Appl. Phys. Lett. **102** (2013).

[21]G. Kochanski and C. Orphanidou, J. Acoust. Soc. Am. **123**, 2780 (2008).

[22]N. Yang, R. Rickard, K. Pluckter, and T. Sulchek, Appl. Phys. Lett. **105** (2014).

[23]F. L. Weng, M. Zhu, and L. Y. Jing, Int. J. Spray Combust. **6**, 247 (2014).

[24]T. C. Lieuwen, J. Propul. Power **18**, 61 (2002).

[25]K. Wang, D. M. Sun, J. Zhang, J. Zou, K. Wu, L. M. Qiu, and Z. Y. Huang, Int. J. Therm. Sci. **94**, 61 (2015).

[26]G. W. Swift, "Thermoacoustics: A unifying perspective for some engines and refrigerators," (J. Acoust. Soc. Am., Sewickley, PA, USA, 2002).

[27]"Matlab r2007b user guides," (The MathWorks Inc., 2007).

[28]J. Smoker, M. Nouh, O. Aldraihem, and A. Baz, J. Appl. Phys. **111**, 104901 (2012).

[29]D. Zhao and Y. Chew, J. Appl. Phys. **112**, 114507 (2012).

[30]L. Fan, Z. Chen, J. J. Zhu, J. Ding, J. Xia, S. Y. Zhang, H. Zhang, and H. Ge, J. Appl. Phys. **117**, 124502 (2015).

[31]L. Fan, S. Y. Zhang, and H. Zhang, J. Appl. Phys. **104**, 113506 (2008).

[32]M. E. H. Tijani, J. C. H. Zeegers, and A. T. A. M. de Waele, J. Appl. Phys. **92**, 2159 (2002).

TABLE CAPTIONS

TABLE I: Geometric parameters of traveling-wave thermoacoustic engine and the grid number used in simulation.

TABLE II: Parameters of mechanical oscillator.

FIGURE CAPTIONS

FIG. 1: Thermoacoustic source and its mechanical partner-a piston-spring oscillator.

FIG. 2: Schematic of discretized equivalent network of the thermoacoustic engine and mechanical oscillator coupled system.

FIG. 3: Free-decay oscillation of thermoacoustic engine when the heating temperature is 292 K (a) Simulation (b) Experiment.

FIG. 4: Beating effect of thermoacoustic source and piston-spring oscillator coupled system when the heating temperature is fixed at 292 K. (a) Simulation (b) Experiment.

FIG. 5: Beating effect of thermoacoustic source and piston-spring oscillator coupled system when the heating temperature is fixed at 353 K. (a) Simulation (b) Experiment.

FIG. 6: Beating effect of thermoacoustic source and piston-spring oscillator coupled system when the heating temperature is fixed at 474 K. (a) Simulation (b) Experiment.

FIG. 7: Indicator diagram $F - X'$ during beating when the heating temperature is 292 K (a) Simulation (b) Experiment. The lines in red denote net positive work is done by the piston while those in blue denote net negative work. First three time intervals of the interactions between thermoacoustic engine and mechanical oscillator are illustrated here, including t_0-t_1, t_1-t_2, and the period after t_2.

FIG. 8: Energy storage levels of the oscillations vs. time at different heating temperatures in simulations.

FIG. 9: Relationships between the beating oscillation frequencies and the resonant frequencies of the thermoacoustic engine and mechanical oscillator. f_1 and f_2 denote the frequencies of the beating oscillation; f_{TE} and f_{MO} are resonant frequencies of thermoacoustic engine and mechanical oscillator, respectively.

FIG. 10: Effects of (a) moving mass M (b) spring stiffness K and (c) resonator length L_r on beating oscillation frequencies when the heating temperature is fixed at 292 K.